High Resolution Dynamics Limb Sounder observations of the gravity wave-driven elevated stratopause in 2006

J. A. France,[1,2] V. L. Harvey,[1,2] M. J. Alexander,[3] C. E. Randall,[1,2] and J. C. Gille[2,4]

Received 17 April 2012; revised 20 July 2012; accepted 8 September 2012; published 23 October 2012.

[1] Temperature observations during January and February 2006 from the High Resolution Dynamics Limb Sounder (HIRDLS), the Microwave Limb Sounder (MLS), and the Sounding of the Atmosphere using Broadband Emission Radiometry (SABER) satellite instruments are compared to illustrate the vertical range over which version 6 HIRDLS temperatures are scientifically useful. In order to determine the quality of HIRDLS temperatures in the middle atmosphere, we compare the height and temperature of the HIRDLS stratopause with MLS and SABER before, during, and after the 2006 major stratospheric sudden warming. Results show that HIRDLS observes the elevated stratopause at 78 km two days later than MLS and five days after SABER. We compare the geographical temperature structure of these data sets at 0.01 hPa during this period. Though HIRDLS temperatures are consistently 5–10 K lower in the mesosphere, this is the first study to show that the horizontal temperature distribution is in good spatial and temporal agreement with MLS and SABER up to ~80 km. Gravity wave momentum flux and planetary wave 1 amplitudes are derived from HIRDLS and shown to be in agreement with previous studies. We use HIRDLS to show a ~30 K increase in stratopause temperature following enhanced gravity wave momentum flux in the lower mesosphere.

Citation: France, J. A., V. L. Harvey, M. J. Alexander, C. E. Randall, and J. C. Gille (2012), High Resolution Dynamics Limb Sounder observations of the gravity wave-driven elevated stratopause in 2006, *J. Geophys. Res.*, *117*, D20108, doi:10.1029/2012JD017958.

1. Introduction

[2] The major Sudden Stratospheric Warming (SSW) event and subsequent reformation of the polar winter stratopause near 0.01 hPa (~80 km) in the Northern Hemisphere (NH) in January 2006 has been well documented [e.g., *Siskind et al.*, 2007; *Manney et al.*, 2008a]. Both models and satellite data have been compared and analyzed to better understand the dynamics that lead to the decent of the stratopause and breakdown of the polar vortex prior to the SSW, and subsequent reformation of the stratopause at high altitudes. Understanding these events is important, as they have been linked to anomalous stratospheric composition. *Randall et al.* [2006] showed that enhanced descent of NO_x into the Arctic vortex occurred after the 2006 SSW, and *Randall et al.* [2009] showed that such enhanced descent coincided with an elevated stratopause in 2006 as well as in other years. It was also shown using satellite observations from the Microwave Limb Sounder (MLS), the Atmospheric Chemistry Experiment - Fourier Transform Spectrometer, and the Sounding of the Atmosphere using Broadband Emission Radiometry (SABER) instrument that there was strong descent of various species, including CO and N_2O, following the reformation of the vortex in 2006 and 2009 [*Manney et al.*, 2008b, 2009a, 2009b; *Lahoz et al.*, 2011]. *Kvissel et al.* [2011] used WACCM to show this CO rich intrusion from the mesosphere into the middle stratosphere is well correlated with the reformation of the vortex in the lower mesosphere. Descent associated with the reformed stratopause was further demonstrated by *Orsolini et al.* [2010], who used water vapor to show that there was anomalously strong descent of dry air from the mesosphere to the stratosphere following the major SSWs of 2004, 2006, and 2009.

[3] Planetary waves have been linked to the large variability in the circumpolar flow that occurs during SSWs [*Matsuno*, 1971; *Andrews et al.*, 1987]. Recent studies using the Whole Atmosphere Community Climate Model (WACCM) have looked at the respective roles of gravity waves (GWs) and planetary waves during elevated stratopause events [*Chandran et al.*, 2011; *Limpasuvan et al.*, 2011]. *Chandran et al.* [2011] and *Limpasuvan et al.* [2011] used WACCM to show that strong planetary wave activity is responsible for the zonal wind reversal and a poleward and downward circulation. The wind reversal results in the filtering of westward-propagating GWs, eastward-propagating GWs propagate through the easterlies associated with the SSW leading to enhanced ascent and

[1]Laboratory for Atmospheric and Space Physics, University of Colorado Boulder, Boulder, Colorado, USA.
[2]Department of Atmospheric and Oceanic Sciences, University of Colorado Boulder, Boulder, Colorado, USA.
[3]Northwest Research Associates, Boulder, Colorado, USA.
[4]National Center for Atmospheric Research, Boulder, Colorado, USA.

Corresponding author: J. A. France, Laboratory for Atmospheric and Space Physics, University of Colorado Boulder, Boulder, CO 80303, USA. (jeffrey.france@colorado.edu)

0148-0227/12/2012JD017958

mesospheric cooling. They show that following the mesospheric cooling, GWs act to reestablish the warm, elevated stratopause. This is consistent with *Siskind et al.* [2007, 2010], who showed that non-orographic GW drag is critical for modeling the reformation and descent of the stratopause following the 2006 SSW, and *Ren et al.* [2011], who used the Canadian Middle Atmosphere Model's data assimilation system to show that the timing and amplitude of the reformation of the stratopause in the mesosphere is sensitive to non-orographic GW drag.

[4] Momentum flux from GWs that propagate from the troposphere to the mesosphere can be derived from the High Resolution Dynamics Limb Sounder (HIRDLS) temperature profiles [*Alexander et al.*, 2008; *Wright et al.*, 2010; *Yan et al.* 2010; *Ern et al.*, 2011]. *Ern et al.* [2011] showed monthly mean January 2006 GW momentum flux (MF) in HIRDLS and SABER, while *Wright et al.* [2010] showed the daily evolution of GW MF at 10 hPa and 60°N from December through April in 2004/2005, 2005/2006, and 2006/2007. These two studies show that, in 2006, GW MF was large during the stratospheric warming and decreased during February. They also showed zonal mean HIRDLS temperatures up to 0.1 hPa on 20 February 2006, which suggests an elevated stratopause. We build upon this work by exploring two months of HIRDLS temperatures up to 80 km. Despite a 5–10 K cold bias above 65 km, HIRDLS captures large-scale geographic temperature structures in the mesosphere and has higher vertical resolution and better spatial sampling than temperature profiles obtained by the MLS and SABER satellite instruments. Previous validation efforts focused on coincident profile comparisons and zonal mean differences. Here we demonstrate for the first time that the large-scale geographic and temporal evolution of mesospheric temperature structures is in agreement with MLS and SABER; we also present an analysis of planetary waves and GWs derived from HIRDLS.

[5] An outline of the paper is as follows. The satellite data and analysis methods are described in section 2. Section 3 shows the evolution of the stratopause in HIRDLS, MLS, and SABER in 2006. The geographic structure of temperature anomalies at 0.01 hPa (∼80 km) is also shown. Section 4 presents planetary wave and GW analysis during January, February, and March 2006. Conclusions are given in Section 5.

2. Data and Analysis Methods

[6] The HIRDLS instrument is an infrared limb-scanning radiometer onboard NASA's Earth Observing System Aura satellite that was launched on 15 July 2004 into a Sun-synchronous polar orbit. On a typical day, there are over 5000 temperature profiles from 65°S to 82°N, which are retrieved using the 15 μm band of CO_2. HIRDLS Version 6 data are used in this work [*Gille et al.*, 2008, 2011]. The vertical resolution of HIRDLS temperatures is 1 km up to 60 km, degrades linearly to 3.5 km at 80 km, the precision is ≤0.5 K in the stratosphere and decreasing to 3 K in the mesosphere; and the accuracy is ≤1 K from 400 hPa to 1 hPa; profiles are spaced 100 km apart along the orbit track [*Gille et al.*, 2011]. According to the HIRDLS data quality document [*Gille et al.*, 2011], version 6 HIRDLS temperatures are scientifically useful up to 0.01 hPa (∼80 km). Note, lower signal-to-noise ratios and biases in the radiances result in a 5–10 K cold bias in the mesosphere compared to lidars, MLS, and SABER observations, and the European Centre for Medium-Range Weather Forecasting assimilated analyses [*Gille et al.*, 2008, 2011]. The Goddard Earth Observing System version 5 (GEOS-5) is used for a priori constraints in the retrieval up to ∼55 km. Data that contain more a priori information than HIRDLS data have a negative precision value and are removed from this work. Previous validation efforts have primarily focused on coincident profile comparisons with sondes and lidars in addition to zonal mean differences with assimilated analyses, MLS, and SABER [*Gille et al.*, 2008, 2011].

[7] The MLS instrument is also onboard the Aura satellite [*Waters et al.*, 2006]. MLS typically measures 3500 temperature profiles between 82°S and 82°N on each day. The profiles are spaced about 165 km apart along the orbit track. Temperature is determined from emissions of oxygen at 118 GHz below 1.41 hPa and at 118 GHz and 190 GHz from 1 hPa to 0.001 hPa [*Schwartz et al.*, 2008]. MLS Version 3.3 data are used in this work. The vertical resolution of MLS temperatures is 4–6 km in the upper stratosphere and lower mesosphere, decreasing to about 7 km around 1 hPa, and to about 10–12 km above 0.01 hPa. The precision is ∼0.6 K in the stratosphere, decreasing to ∼2.5 K in the mesosphere; there is an up to 8 K cold bias in the mesosphere [*Livesey et al.*, 2011]. Version 3.3 MLS temperatures are deemed scientifically useful up to ∼90 km and have been filtered using the precision, status, quality, and convergence values provided by the MLS science team [*Livesey et al.*, 2011].

[8] SABER was launched onboard the Thermosphere Ionosphere Mesosphere Energetics and Dynamics (TIMED) satellite on 7 December 2001 into a 625 km circular orbit with an inclination of 74.1° [*Russell et al.*, 1999]. SABER samples approximately every 300 km along the orbit track and provides coverage from 52°S to 83°N, or from 83°S to 52°N, depending on the orientation of TIMED. The coverage alternates every 60 days due to yaw maneuvers of TIMED that rotate the SABER view direction by 180°. SABER data products are reported on 201 geometric altitude levels ranging from 0 to 200 km in 1 km increments. The vertical resolution of SABER is 2–3 km [*Mertens et al.*, 2001]. This work uses version 1.07 kinetic temperature and derived geopotential height as a function of pressure provided in the L2A data files obtained from http://saber.gats-inc.com/. Kinetic temperature is determined from the 15 μm and 4.3 μm bands of CO_2 with the assumptions that CO_2 is well mixed and has a well-known volume mixing ratio. *Remsberg et al.* [2008] compared the SABER version 1.07 temperatures to data from the Michelson Interferometer for Passive Atmospheric Sounding (MIPAS) and Rayleigh lidar profiles for the upper stratosphere and lower to middle mesosphere, and found that SABER has a 1 K cold bias near the stratopause. They determined the projected error for SABER in the upper stratosphere and lower mesosphere from systematic and random errors to be ±2 K.

[9] For this work, we define the stratopause simply as the temperature maximum between 20 km and 90 km. To explore the geographic temperature structure, daily profiles for each data set are gridded onto a 5° latitude by 5° longitude grid by applying a spatial Delaunay Triangulation at each vertical level. To ensure differentiability, a distance weighted smoothing is applied to the resulting grid. The data are

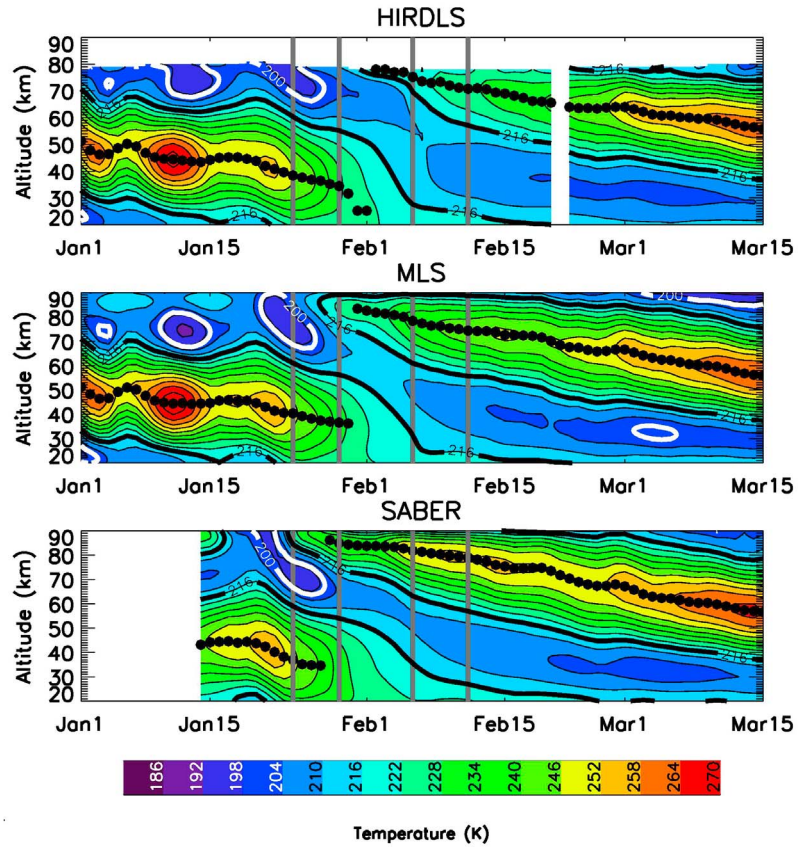

Figure 1. Time-altitude plot of daily average temperature poleward of 75°N from 1 January to 15 March 2006 from 20 km to 90 km for (top) HIRDLS, (middle) MLS, and (bottom) SABER. The black dots denote the stratopause. The 200 and 216 K isotherms are shown by the thick white and black contours, respectively. Vertical gray lines indicate 24 January, 29 January, 6 February, and 12 February. White regions represent missing data.

then fit to a 0.2 km vertical grid from 15 to 90 km using a 6th-order polynomial similar to the method developed by *McDonald et al.* [2011] and used by *Day et al.* [2011].

3. The Elevated Stratopause in 2006

[10] Figure 1 shows the mean temperature poleward of 75°N for HIRDLS, MLS, and SABER as a function of altitude and time from 1 January 2006 to 15 March 2006. The black dots denote the stratopause. Vertical gray lines indicate 24 January, 29 January, 6 February, and 12 February; the vertical and horizontal temperature distribution on these days will be shown in Figures 3 and 4, respectively. HIRDLS and MLS show that near 50 km, there are warm events on 2, 11, and 22 January and associated cold events near 80 km. Because of the spacecraft yaw, SABER alternates between viewing the Arctic and Antarctic regions; observations in the Arctic begin on 14 January. Between 23 and 25 January, all three data sets show the stratopause descending below 40 km. From 24 January to 6 February, the stratopause is not well defined as the atmosphere is nearly isothermal between 25 km and 55 km; this increases the sensitivity of the stratopause algorithm to small local temperature maxima within the near-isothermal layer. In early February, all three instruments observe a warm layer above 70 km that gradually descends to ~55 km by 15 March. In SABER and MLS the elevated stratopause is first observed at 84 km on 28 January and at 81 km on 31 January, respectively. HIRDLS first observes the elevated stratopause on 2 February, and the temperature at the stratopause in SABER, MLS, and HIRDLS is 238 K, 225 K, and 226 K, and the height is 84 km, 82 km, and 78 km, respectively. The lack of a high stratopause in HIRDLS before 2 February is primarily because the stratopause is at an altitude above where HIRDLS data are useful. In late February and early March, when the stratopause is located below 70 km, differences in the height and temperature of the stratopause among the instruments are less than 3 km and 6 K, respectively. Figure 1 is consistent with previous work by *Manney et al.* [2008a] and *Orsolini et al.* [2010]. *Manney et al.* [2008a, Figure 3] showed zonal mean temperature observations at 70°N from SABER and MLS during December 2005 through March 2006, and found that the stratopause reforms at ~0.01 hPa near the beginning of February. *Orsolini et al.* [2010, Figure 2] used data poleward of 70°N from the Sub-Millimeter Radiometer onboard the Odin satellite to show a reformed stratopause near 0.01 hPa (~80 km) and 225 K in early February.

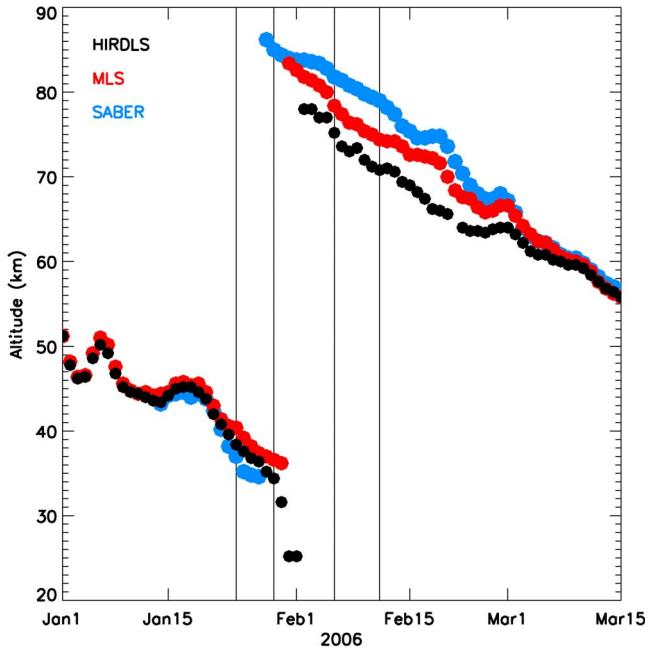

Figure 2. Time series of stratopause height as shown in Figure 1. The stratopause observed by HIRDLS, MLS, and SABER is indicated by the black, red, and blue dots, respectively.

[11] Figure 2 shows a time series of the stratopause height in each data set for the same date range shown in Figure 1. At the onset of the SSW (24 January, indicated by first vertical line), all three data sets show the ~10 km descent of the stratopause within one day of each other. The stratopause is near 30–40 km for about one week during the SSW. The stratopause observed by HIRDLS on 2 February is 5 km below the stratopause observed by SABER and 2 km below that observed by MLS. The MLS mesospheric cold bias combined with its coarse vertical resolution likely contributes to observing the elevated stratopause at a later date and lower altitude than SABER. Likewise, the low bias in HIRDLS temperatures in the mesosphere combined with the 80 km upper limit is responsible for the delay in HIRDLS capturing the elevated stratopause. The fact that both MLS and HIRDLS show the stratopause at lower altitude indicates that the low temperature bias in these instruments with respect to SABER is a more important factor than the resolution. As the elevated stratopause first descends, HIRDLS is in excellent agreement with MLS; the stratopause from each of these instruments is ~4–10 km lower than that measured by SABER. In early to mid-February, both HIRDLS and MLS observe the stratopause descending more rapidly than that in the SABER observations. In late February and early March, when the stratopause is located below 70 km, differences in the height of the stratopause among the instruments are less than 3 km.

[12] Figure 3 shows HIRDLS, MLS, and SABER zonal mean temperatures in the NH on the four days indicated by the vertical lines in Figures 1 and 2. On 24 January, the low stratopause is evident in all three data sets at high northern latitudes. Near 80–90 km and poleward of ~60°N, there is a pronounced warm layer in the SABER data; a warm layer is present in the MLS data as well, but it is not as pronounced. On 29 January, the elevated warm layer begins to appear in the HIRDLS data; by this time, it is much more pronounced in both the MLS and SABER data. On this day, the polar stratopause is identified at high altitudes in SABER, but is still at low altitudes in HIRDLS and MLS. The elevated polar warm layer that is observed by MLS and HIRDLS on this day was not demarked as the stratopause because it is a local maximum, while the higher temperatures in the lower stratosphere are considered to be the stratopause. By 6 February, the stratopause is located above 75 km in all three data sets. While in good qualitative agreement, the elevated stratopause is highest and warmest in SABER and lowest and coldest in HIRDLS. On 12 February, the latitudinal extent of the elevated stratopause is in excellent agreement among the data sets; however, the polar stratopause observed by SABER is ~5 K warmer and ~2–3 km higher than MLS, and 10 K warmer and 6–8 km higher than HIRDLS. Differences between HIRDLS and SABER are likely due to the low bias in HIRDLS mesospheric temperatures.

3.1. Geographic Temperature Distributions

[13] Figure 4 shows the horizontal temperature anomaly structure in the NH at 0.01 hPa (~80 km) for HIRDLS, MLS, and SABER for the same dates shown in Figure 3. We subtract the zonal mean temperature from each latitude band in order to reduce instrument biases. This allows us to more directly compare the geographical temperature distribution as well as the magnitude of features observed by each instrument. This figure shows for the first time that HIRDLS captures large-scale geographic structure observed by MLS and SABER at mesospheric altitudes. On 24 January, the anomalous temperature structure is in good agreement among the data sets. A cold anomaly is evident in all three data sets between 40 and 60°N and centered over the Greenwich Meridian. A warm anomaly centered over Canada is also evident in all three data sets, though it has a larger magnitude in MLS and HIRDLS than in SABER. The region of highest temperature anomalies spirals to the southwest from Canada over the North Pacific, Asia, Europe, and Northern Africa. On 29 January the cold anomaly has shifted slightly poleward in all three data sets, and the warm anomaly is visible near the western coast of North America. On 6 February, the regions covered by the warm and cold anomalies are generally smaller and the cold anomalies are also weaker. All three do show a weak cold anomaly in the Atlantic between 40 and 50°N, and a warm anomaly over Canada. On 12 February a strong cold anomaly over Siberia and a warm anomaly in northwestern Canada and Alaska are shown in all three data sets. For the days shown (as well as days not shown), the geographic pattern in HIRDLS temperature anomalies agrees well with that observed by MLS and SABER. Taken together, the results here provide compelling evidence that HIRDLS temperatures can be used to investigate meteorological phenomena in the mesosphere.

4. Planetary and Gravity Wave Analysis

[14] Having shown that HIRDLS effectively represents the major SSW of January 2006, we take advantage of the

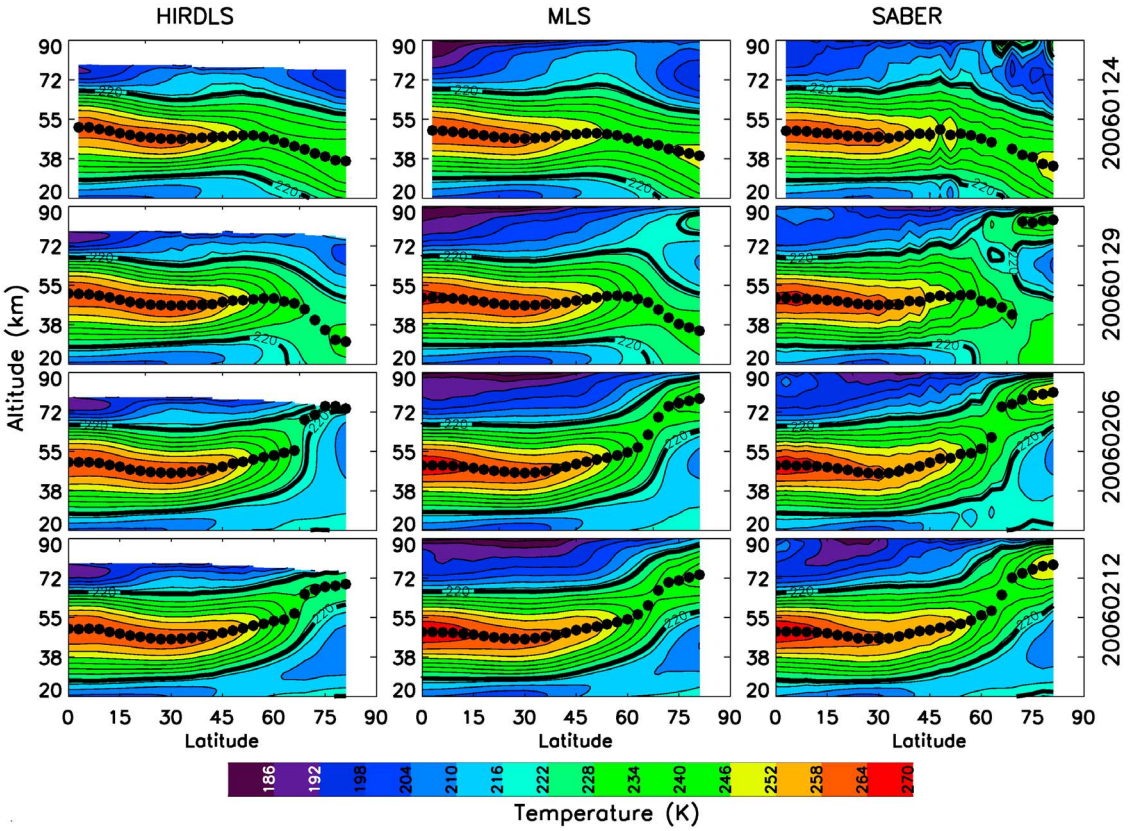

Figure 3. Daily zonal mean temperatures for (left) HIRDLS, (middle) MLS, and (right) SABER in 2006 on 24 January, 29 January, 6 February, and 12 February. The black dots represent the stratopause. Temperature profiles are binned in 2.5° latitude bins. The thick black line is the 220 K isotherm.

data's high vertical and temporal resolution to derive planetary and gravity wave diagnostics.

4.1. Planetary Wave Analysis

[15] Figure 5 shows a time-altitude section of the daily amplitude of planetary wave 1 in geopotential height at 60°N from 1 January through 15 March 2006 based on (a) HIRDLS, (b) MLS, and (c) SABER. These amplitudes were determined by fitting a sine wave to the daily mean geopotential height data from each instrument around the 57–63°N latitude band. The amplitude of the sine wave is considered the wave 1 height amplitude. The daily average stratopause poleward of 75°N is indicated by the white dots. The vertical gray line depicts 8 January when there is a maximum in planetary wave amplitudes in both instruments. HIRDLS is in good agreement with MLS and SABER, and all three instruments are in good agreement with *Siskind et al.* [2010, Figure 1f], who used the Navy Operational Global Atmospheric Prediction System Advanced-Level Physics High-Altitude (NOGAPS-ALPHA) model. The time-altitude evolution of planetary wave 1 amplitudes is also consistent with results from *Manney et al.* [2008a, Figure 3], who showed wave 1 amplitudes at 60°N using MLS, SABER, GEOS-5 [*Rienecker et al.*, 2007], and the European Centre for Medium-Range Weather Forecasting (ECMWF) [*Simmons et al.*, 2005]. In early to mid-January, planetary wave 1 amplitudes are large at the stratopause. During the SSW in late January (when the stratopause descends), planetary wave amplitudes decrease in the stratosphere. In February following the SSW, large planetary wave amplitudes are co-located with the descending elevated stratopause, consistent with *Manney et al.* [2008a]. These results confirm the WACCM model results in *Limpasuvan et al.* [2011], who showed that the planetary wave 1 forcing contributes to the reformation and initial descent of the stratopause.

4.2. Gravity Wave Analysis

[16] GW MF is derived from HIRDLS version 6 temperature profiles using the method described by *Alexander et al.* [2008]. The method uses the S-transform [*Stockwell et al.*, 1996], which is a Fourier analysis that also gives localization of spectral properties similar to a wavelet analysis, but with an absolute phase reference. Gravity wave temperature perturbations are first isolated by subtracting a background temperature representing the large-scale planetary wave temperature features. This background is defined with an S-transform analysis in the zonal direction using HIRDLS temperatures binned in 2.5-degree latitude bins. The zonal wave number 1–5 features in the transform define the background. We calculate the gravity waves by subtracting the background temperature from the individual HIRDLS temperature profiles. We then perform an S-transform analysis in the vertical on each profile and compute the covarying spectrum between adjacent temperature perturbation profiles along the measurement track. The vertical wavelength

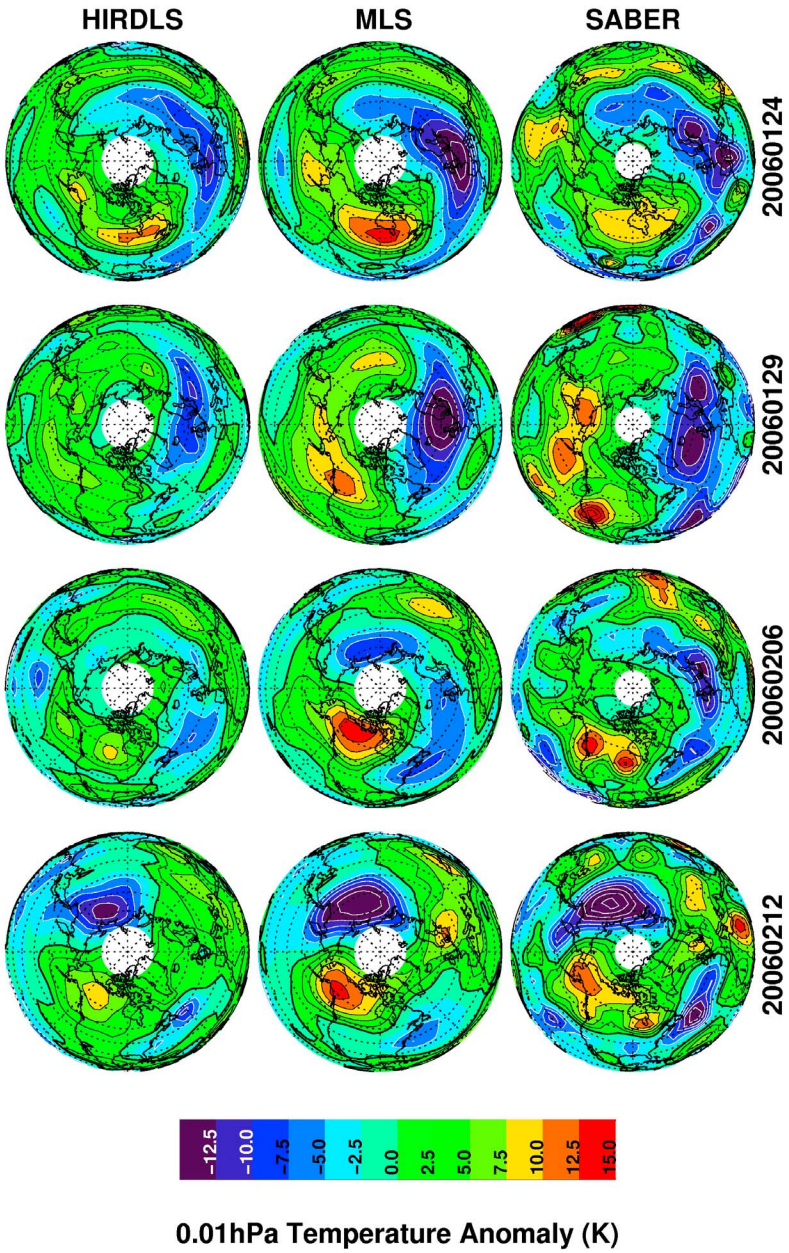

Figure 4. NH polar orthographic plots of daily mean gridded temperature minus the zonal mean at 0.01 hPa on 24 Jan (first row), 29 Jan (second row), 6 Feb (third row), and 12 Feb (fourth row).

and amplitude at the peak in the covariance spectrum is determined for each profile pair as a function of height. The covarying S-Transform also gives a wave phase shift for this peak across the horizontal distance between the profile pairs, and this is used to estimate horizontal wavelength. Combining these three parameters (vertical and horizontal wavelength and temperature amplitude) allows an estimate of MF as a function of height along the HIRDLS measurement track [e.g., *Alexander et al.*, 2008, equation (6)]. It should be noted that true MF is a vector with direction given by the horizontal wave number vector, whereas with HIRDLS we can only estimate the along-track component of the horizontal wave number. The limited spatial sampling also sometimes subsamples the true horizontal wavelength. Thus, the horizontal wavelength is generally biased long, and the MF estimated from HIRDLS correspondingly biased low. Despite these limitations, HIRDLS has the best combined horizontal plus vertical resolution of any limb-sounding satellite measurement to date. The results include gravity waves with vertical wavelengths ranging from 4 to 25 km and horizontal wavelengths longer than 200 km.

[17] Although MLS and SABER have longer-term data records, HIRDLS has twice the resolution in both the horizontal and vertical than the next best limb-viewing measurements from SABER, making it superior for any short-term GWs studies during the three-year period of HIRDLS data. Thus the following GW analysis will be based solely on HIRDLS. We limit our GW analysis to below 55 km, because

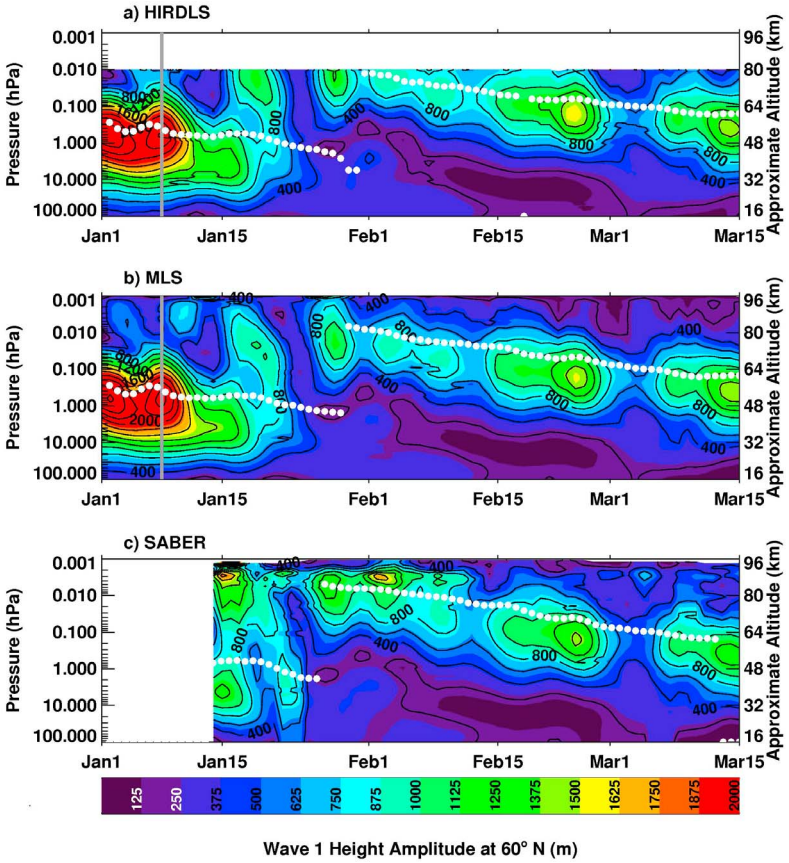

Figure 5. Time series of daily averaged zonal mean wave 1 geopotential height amplitudes between 57°N and 63°N for (a) HIRDLS, (b) MLS, and (c) SABER. The daily average stratopause poleward of 75°N is indicated by the white dots.

noise in HIRDLS temperatures increases above 60 km, and HIRDLS ability to quantify gravity waves above that altitude has not yet been validated. Figure 6a shows time-altitude sections of HIRDLS daily averaged zonal mean GW MF. The daily average stratopause between 70 and 82°N is indicated by the white dots. The gray line depicts 8 January and is co-located with a maximum in GW MF at all altitudes below 50 km. White contours in (a) are the zonal mean zonal wind from GEOS-5 poleward of 70°N latitude. Figure 6a shows that the observed wind and GW MF observed by HIRDLS poleward of 70°N is in agreement with what *Wright et al.* [2010, Figure 7] showed using HIRDLS MF and ECMWF winds at 60°N. They found that when zonal mean winds become easterly in late-January, there is a decrease in GW MF, consistent with filtering of the GWs by the easterly winds. This reduction persists until the zonal mean winds become westerly in mid-February. We show that the winds and GW MF between 70 and 82°N are consistent with what is shown at 60°N by *Wright et al.* [2010]. Thus, following the wind reversal in late January, GW MF was not only reduced near the vortex edge, but throughout the polar region as well.

[18] Figure 6b shows a latitude-time section of HIRDLS MF divided by density, or kinematic momentum flux (KMF), consistent with Figure 6a. White contours indicate mean temperature between 70 and 82°N. Since GW MF is proportional to atmospheric density, MF in the mesosphere is relatively small compared with the lower stratosphere, so dividing by density will emphasize the influence of GWs in regions of lower atmospheric density. HIRDLS temperature is shown using white contours. There is an increase in GW KMF beginning on 5 January that maximizes on 8 January, which extends from the lower stratosphere to the lower mesosphere. The largest amplitudes of GW KMF on this date occur in the lower mesosphere. The temperature contours indicate an increase in temperature at the stratopause following the increase in GW KMF between 5 and 8 January. The relationship between GW MF and temperature has been described by *Chandran et al.* [2011, Figure 1]. Using WACCM, they showed that following easterly GW forcing in the mesosphere, there is enhanced adiabatic descent in the stratosphere and adiabatic ascent in the mesosphere, resulting in a warming of the stratosphere and a cooling of the mesosphere. Our results support this mechanism. HIRDLS temperatures show a ~30 K temperature increase at the stratopause that occurs within 3 days of the maximum GW KMF in the lower mesosphere. Following the SSW, GW KMF in the mesosphere is westerly due to filtering by easterly winds in the stratosphere. *Limpasuvan et al.* [2011] used the WACCM model to show that westerly GW MF plays a

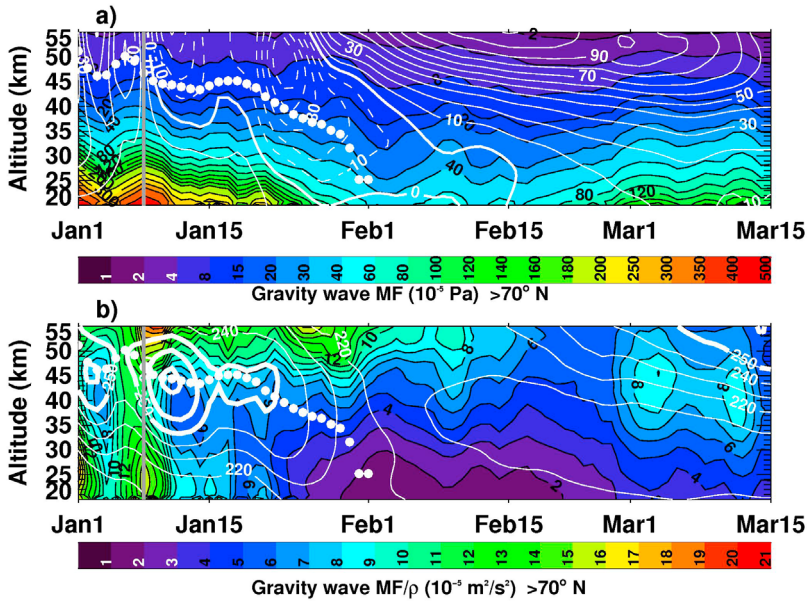

Figure 6. Time series of daily averaged zonal mean GW (a) momentum flux and (b) kinematic momentum flux poleward of 70°N latitude band for HIRDLS. The daily average stratopause poleward of 70°N is indicated by the white dots. White contours are (a) GEOS-5 zonal mean zonal wind, and (b) HIRDLS temperature. Thick white contours emphasize temperatures greater than 250 K.

critical role in re-establishing the westerly polar night jet. This leads to a poleward residual circulation and the reformation of the stratopause in the mesosphere.

5. Conclusions

[19] This is the first work to show that, while there is a significant cold bias in the mesosphere, the geographic structure in mesospheric temperature observed by HIRDLS near 80 km is in good agreement with MLS and SABER. We use the major SSW in January 2006 and subsequent reformation of the stratopause at high altitudes as a case study to demonstrate the utility of HIRDLS temperature data at mesospheric altitudes. During the period studied, HIRDLS captures the evolution of the stratopause and is consistent with MLS and SABER once the stratopause descends below 78 km, which is the first measurement of the stratopause below the upper altitude limit of HIRDLS temperatures. The elevated stratopause was first observed at different altitudes, with different temperatures, and on different dates by the three instruments. The relative timing of the stratopause reformation and its temperature is largely explained by differences in vertical range of the instruments, as well as the low temperature bias in HIRDLS and MLS with respect to SABER. Significantly, we show that HIRDLS accurately represents the daily large-scale geographic temperature anomaly pattern at 0.01 hPa (~80 km), and the evolution of mesospheric temperature anomalies before, during, and after the January 2006 SSW.

[20] Planetary wave 1 amplitudes in geopotential height are shown at 60°N. The altitude-time structure in HIRDLS is in good agreement with previous work using NOGAPS-ALPHA, WACCM, GEOS-5, ECMWF, SABER, and MLS. HIRDLS GW MF is also shown to be consistent with recent studies using WACCM to understand the role of GWs during SSWs. HIRDLS offers near-global data with higher vertical resolution and higher spatial sampling than MLS and SABER. As a result, it can be used to supplement these data sets and provide an additional source of temperature data for mesospheric analyses.

[21] **Acknowledgments.** We thank the HIRDLS, MLS, and SABER science teams for the satellite data. We thank Matthias Brakebusch for the gridding routine. The authors acknowledge support from the United States National Science Foundation under grants ARC 1107498 and AGS 0940124. This work was supported by NASA grants NNX10AQ54G and NAS5-97046. Support for M.J.A. is from the NASA Atmospheric Chemistry Program–Aura Science Team contract NNH11CD32C. The National Center for Atmospheric Research is sponsored by the National Science Foundation.

References

Alexander, M. J., et al. (2008), Global estimates of gravity wave momentum flux from High Resolution Dynamics Limb Sounder (HIRDLS) observations, *J. Geophys. Res.*, *113*, D15S18, doi:10.1029/2007JD008807.

Andrews, D. G., J. R. Holton, and C. B. Leovy (1987), *Middle Atmosphere Dynamics*, Academic, Orlando, Fla.

Chandran, A., R. L. Collins, R. R. Garcia, and D. R. Marsh (2011), A case study of an elevated stratopause generated in the Whole Atmosphere Community Climate Model, *Geophys. Res. Lett.*, *38*, L08804, doi:10.1029/2010GL046566.

Day, K. A., R. E. Hibbins, and N. J. Mitchell (2011), Aura MLS observations of the westward-propagating s = 1, 16-day planetary wave in the stratosphere, mesosphere and lower thermosphere, *Atmos. Chem. Phys.*, *11*, 4149–4161, doi:10.5194/acp-11-4149-2011.

Ern, M., et al. (2011), Implications for atmospheric dynamics derived from global observations of gravity wave momentum flux in stratosphere and mesosphere, *J. Geophys. Res.*, *116*, D19107, doi:10.1029/2011JD015821.

Gille, J., et al. (2008), High Resolution Dynamics Limb Sounder: Experiment overview, recovery, and validation of initial temperature data, *J. Geophys. Res.*, *113*, D16S43, doi:10.1029/2007JD008824.

Gille, J., et al. (2011), High resolution dynamics limb sounder Earth Observing System (EOS) data description and quality version 6(V6), Rep. SC–HIR–1511 F, Univ. of Colo. and Natl. Cent. for Atmos. Res., Boulder, Colo. [available at http://www.eos.ucar.edu/hirdls/data/products/HIRDLS-DQD_V6-1.pdf.]

Kvissel, O. K., et al. (2011), Mesospheric intrusion and anomalous chemistry during and after a major stratospheric sudden warming, *J. Atmos. Sol. Terr. Phys.*, *78–79*, 116–124, doi:10.1016/j.jastp.2011.08.015.

Lahoz, W. A., Q. Errera, S. Viscardy, and G. L. Manney (2011), The 2009 stratospheric major warming described from synergistic use of BASCOE water vapour analyses and MLS observations, *Atmos. Chem. Phys.*, *11*, 4689–4703, doi:10.5194/acp-11-4689-2011.

Limpasuvan, V., et al. (2011), The roles of planetary and gravity waves during a major stratospheric sudden warming as characterized in WACCM, *J. Atmos. Sol. Terr. Phys.*, *78–79*, 84–98, doi:10.1016/j.jastp.2011.03.004.

Livesey, N. J., et al. (2011), EOS MLS Version 3.3 level 2 data quality and description document, *Tech. Rep. D-16159*, Jet Propul. Lab., Pasadena, Calif. [Available at http://mls.jpl.nasa.gov.]

Manney, G. L., et al. (2008a), The evolution of the stratopause during the 2006 major warming: Satellite data and assimilated meteorological analyses, *J. Geophys. Res.*, *113*, D11115, doi:10.1029/2007JD009097.

Manney, G. L., et al. (2008b), The high Arctic in extreme winters: Vortex, temperature, and MLS and ACE-FTS trace gas evolution, *Atmos. Chem. Phys.*, *8*, 505–522, doi:10.5194/acp-8-505-2008.

Manney, G. L., et al. (2009a), Satellite observations and modeling of transport in the upper troposphere through the lower mesosphere during the 2006 major stratospheric sudden warming, *Atmos. Chem. Phys.*, *9*, 4775–4795, doi:10.5194/acp-9-4775-2009.

Manney, G. L., et al. (2009b), Aura Microwave Limb Sounder observations of dynamics and transport during the record-breaking 2009 Arctic stratospheric major warming, *Geophys. Res. Lett.*, *36*, L12815, doi:10.1029/2009GL038586.

Matsuno, T. (1971), A dynamical model of the stratospheric sudden warming, *J. Atmos. Sci.*, *28*, 1479–1494, doi:10.1175/1520-0469(1971)028<1479:ADMOTS>2.0.CO;2.

McDonald, A. J., R. E. Hibbins, and J. M. Jarvis (2011), Properties of the quasi-16 day wave derived from EOS MLS observations, *J. Geophys. Res.*, *116*, D06112, doi:10.1029/2010JD014719.

Mertens, C., et al. (2001), Retrieval of mesospheric and lower thermospheric kinetic temperature from measurements of CO_2 15 micron Earth limb emission under non-LTE conditions, *Geophys. Res. Lett.*, *28*(7), 1391–1394, doi:10.1029/2000GL012189.

Orsolini, Y. J., J. Urban, D. P. Murtagh, S. Lossow, and V. Limpasuvan (2010), Descent from the polar mesosphere and anomalously high stratopause observed in 8 years of water vapor and temperature satellite observations by the Odin Sub- Millimeter Radiometer, *J. Geophys. Res.*, *115*, D12305, doi:10.1029/2009JD013501.

Randall, C. E., et al. (2006), Enhanced NO_x in 2006 linked to strong upper stratospheric Arctic vortex, *Geophys. Res. Lett.*, *33*, L18811, doi:10.1029/2006GL027160.

Randall, C. E., V. L. Harvey, D. E. Siskind, J. France, P. F. Bernath, C. D. Boone, and K. A. Walker (2009), NO_x descent in the Arctic middle atmosphere in early 2009, *Geophys. Res. Lett.*, *36*, L18811, doi:10.1029/2009GL039706.

Remsberg, E. E., et al. (2008), Assessment of the quality of the Version 1.07 temperature versus pressure profiles of the middle atmosphere from TIMED/SABER, *J. Geophys. Res.*, *113*, D17101, doi:10.1029/2008JD010013.

Ren, S., S. Polavarapu, S. R. Beagley, Y. Nezlin, and Y. J. Rochon (2011), The impact of gravity wave drag on mesospheric analyses of the 2006 stratospheric major warming, *J. Geophys. Res.*, *116*, D19116, doi:10.1029/2011JD015943.

Rienecker, M. M., et al. (2007), The GEOS data assimilation system–Documentation of versions 5.0.1 and 5.1.0, *NASA Tech. Memo.*, *TM-2007–104606*, 92 pp.

Russell, J. M., III, M. G. Mlynczak, L. L. Gordley, J. Tansock, and R. Esplin (1999), An overview of the SABER experiment and preliminary calibration results, *Proc. SPIE Int. Soc. Opt. Eng.*, *3756*, 277–288.

Schwartz, M. J., et al. (2008), Validation of the Aura Microwave Limb Sounder temperature and geopotential height measurements, *J. Geophys. Res.*, *113*, D15S11, doi:10.1029/2007JD008783.

Simmons, A. J., M. Hortal, G. Kelly, A. McNally, A. Untch, and S. Uppala (2005), ECMWF analyses and forecasts of stratospheric winter polar vortex break-up: September 2002 in the southern hemisphere and related events, *J. Atmos. Sci.*, *62*, 668–689, doi:10.1175/JAS-3322.1.

Siskind, D. E., et al. (2007), On recent interannual variability of the Arctic winter mesosphere: Implications for tracer descent, *Geophys. Res. Lett.*, *34*, L09806, doi:10.1029/2007GL029293.

Siskind, D. E., S. D. Eckermann, J. P. McCormack, L. Coy, K. W. Hoppel, and N. L. Baker (2010), Case studies of the mesospheric response to recent minor, major, and extended stratospheric warmings, *J. Geophys. Res.*, *115*, D00N03, doi:10.1029/2010JD014114.

Stockwell, R. G., L. Mansinha, and R. P. Lowe (1996), Localisation of the complex spectrum: The S-transform, *IEEE Trans. Signal Process.*, *44*(4), 998–1001, doi:10.1109/78.492555.

Waters, J. W., et al. (2006), The Earth Observing System Microwave Limb Sounder (EOS MLS) on the Aura satellite, *IEEE Trans. Geosci. Remote Sens.*, *44*, 1075–1092, doi:10.1109/TGRS.2006.873771.

Wright, C. J., et al. (2010), High Resolution Dynamics Limb Sounder measurements of gravity wave activity in the 2006 Arctic stratosphere, *J. Geophys. Res.*, *115*, D02105, doi:10.1029/2009JD011858.

Yan, X., N. Arnold, and J. J. Remedios (2010), Global observations of gravity waves from High Resolution Dynamics Limb Sounder temperature measurements: A yearlong record of temperature amplitude and vertical wavelength, *J. Geophys. Res.*, *115*, D10113, doi:10.1029/2008JD011511.